Hill, J.G., Mitrushchenkov, A.O., and Peterson, K.A. (2013) Ab initio ro-vibrational spectroscopy of the group 11 cyanides: CuCN, AgCN, and AuCN. Journal of Chemical Physics, 138 (13). 134314. ISSN 0021-9606

A copy can be downloaded for personal non-commercial research or study, without prior permission or charge

Content must not be changed in any way or reproduced in any format or medium without the formal permission of the copyright holder(s)

When referring to this work, full bibliographic details must be given

http://eprints.gla.ac.uk/76832/

Deposited on: 11 April 2013

Enlighten – Research publications by members of the University of Glasgow
http://eprints.gla.ac.uk

Ab initio ro-vibrational spectroscopy of the group 11 cyanides: CuCN, AgCN, and AuCN

J. Grant Hill[†]

School of Chemistry, Joseph Black Building, University of Glasgow, Glasgow G12 8QQ, U.K.

Alexander O. Mitrushchenkov

Université Paris-Est, Laboratoire Modélisation et Simulation Multi Echelle, MSME UMR 8208 CNRS, 5 bd Descartes, 77454 Marne-la-Vallée, France

Kirk A. Peterson

Department of Chemistry, Washington State University, Pullman, Washington 99164

Abstract

Accurate near-equilibrium potential energy and dipole moment functions have been calculated for the linear coinage-metal cyanides CuCN, AgCN, and AuCN using coupled cluster methods and sequences of correlation consistent basis sets. The explicitly correlated CCSD(T)-F12b method is used for the potential energy surfaces (PESs) with inclusion of core correlation, and is combined with contributions from molecular spin-orbit coupling, scalar relativity, and effects due to higher order electron correlation. The resulting composite PESs are used in both perturbative and variational calculations of the ro-vibrational spectra. In addition to accurate equilibrium geometries, the ro-vibrational spectra are predicted, which are found to be relatively intense in the 200 - 600 cm^{-1} range due to the bending and metal-carbon stretching modes. The CN stretch near 2165 cm^{-1} is also predicted to carry enough intensity to allow its observation by experiment. A strong Fermi-resonance is predicted between the first overtone of the bend and the fundamental of the metal-carbon stretch for both CuCN and AgCN. The heats of formation at 0 K are predicted from their calculated atomization energies to be 89.8, 88.6, and 104.5 kcal mol^{-1} for CuCN, AgCN, and AuCN, respectively.

[†] email addresses: *grant.hill@glasgow.ac.uk, Alexander.Mitrushchenkov@univ-mlv.fr, kipeters@wsu.edu*

I. INTRODUCTION

The group 11 metal cyanides have a number of chemical uses, including the role of CuCN as a reagent in the selective formation of C–C and C–Si bonds (see Ref. 1), as intermediates in the MacArthur-Forrest process of mining (see Ref. 2 and references therein), and the relation of AuCN to $[Au(CN)_2]^-$, which is used in gold production. There is also interest in the qualitative description of the nature of the M–CN bond. Both experimental and theoretical studies agree that the Au–C bond is shorter and stronger than Ag–C, with photoelectron velocity map imaging studies[3] indicating that the Cu–C bond is slightly weaker than that in Au–C. While the work of Frenking and co-workers[4] have interpreted the bonding as being predominately ionic (M^+-CN^-) with only small contributions from π bonding, some debate still remains as to the bonding character, particularly in AuCN. Zaleski-Ejgierd et al.[5] reasoned that as the theoretical Au–C bond distance is only slightly larger than the sum of the triple-bond covalent radii, this bond should be classified as a multiple-bond, whilst Wu et al.[3] used a frontier orbital analysis to show that there is little back donation from the metal and argue that the Au–C bond is simply a short single bond. Wu et al.[3] also carried out a natural bond orbital analysis that indicated Cu–CN and Ag–CN can be described as ionic bonding, whilst Au–CN is covalently bound, in line with their experimental electron affinities.

Experimental data on the monomeric gas-phase group 11 cyanides have been produced using microwave spectroscopy,[6,7] photoelectron spectroscopy,[8] and photoelectron velocity-map imaging[3] as mentioned above. These experiments have yielded accurate rotational constants, estimates of some of the vibrational frequencies, and their electron affinities. The highest level theoretical study reported in the literature to date on all three molecules utilized the coupled cluster with singles, doubles and perturbative triples [CCSD(T)] method, along with quadruple-zeta quality basis sets and a correction for spin-orbit (SO) effects.[5] CuCN was also compared to the CuNC isomer at the CCSD(T) level using scalar relativistic effects, with the former found to be 11.5 kcal mol^{-1} lower in energy.[9] These studies have superseded a number of earlier, somewhat lower-level calculations,[4,10-12] although all are in agreement that these molecules are linear with $^1\Sigma^+$ electronic ground states.

High-accuracy theoretical calculations on transition metal containing species have traditionally been regarded as significantly more demanding than those on equivalently sized molecules made up of main group elements. This is due to a number of factors, including the number of electrons present, the greater likelihood of multireference character, the importance of relativistic effects, and the observed slower convergence with respect to basis set size. The development of systematically convergent, correlation consistent basis sets paired with relativistic pseudopotentials (PPs) has gone some way to remedying these problems for single reference cases, but until recently slow convergence has restricted the ultimate accuracy of wavefunction-based calculations on transition metals. The advent of explicitly correlated methods (for recent reviews of explicitly correlated methods, see Ref. 13), particularly the CCSD(T)-F12b method,[14,15] where the basis set size required to reach a desired accuracy is greatly reduced, has the implication that high-accuracy investigations of ab initio spectroscopy and thermochemistry can now be carried out on a significantly wider range of systems. By utilizing compact auxiliary basis sets specifically designed to produce well-controlled errors in F12 calculations, the present work demonstrates that CCSD(T)-F12b calculations, as part of a composite protocol, can be used on transition metal containing species to produce high accuracy potential energy surfaces (PESs) and spectroscopic properties that are in excellent agreement with published experimental data. Composite PESs calculated for CuCN, AgCN, and AuCN, combined with dipole moment functions, have been employed in this work in vibrational perturbation theory and variational nuclear motion calculations to produce ro-vibrational spectroscopic constants. Accurate thermodynamic properties of these molecules, namely atomization and formation enthalpies, have also been calculated.

II. METHODOLOGY

Near-equilibrium potential energy surfaces (PESs) were calculated using a composite approach for a total of 50 symmetry unique points on the PES of each molecule in the internal coordinates r_1 (metal to carbon distance), r_2 (C-N distance), and θ (bond angle). These geometries approximately covered the ranges $-0.3\ a_o \leq r_1 - r_{1e}, r_2 - r_{2e} \leq +0.5\ a_o$ and $140^o \leq \theta \leq 180^o$. For CuCN and AgCN each point on the PES was evaluated as:

$$E(r_1, r_2, \theta) = \mathrm{CCSD(T)} + \Delta\mathrm{CV} + \Delta\mathrm{DK} + \Delta\mathrm{HC} + \Delta\mathrm{SO}\,, \qquad (1)$$

where ΔCV is a correction for the correlation of outer-core electrons, ΔDK accounts for the residual scalar relativistic effects using the Douglas-Kroll-Hess (DKH) Hamiltonian,[16] ΔHC is a correction for higher level electron correlation effects beyond CCSD(T), and ΔSO accounts for molecular spin-orbit coupling. The composite energy for AuCN was slightly modified to be:

$$E(r_1, r_2, \theta) = \mathrm{CCSD(T)} + \Delta\mathrm{CV} + \Delta\mathrm{DK} + \Delta 4f + \Delta\mathrm{HC} + \Delta\mathrm{SO}\,, \qquad (2)$$

where $\Delta 4f$ is the effect of correlating the $4f$ electrons on Au.

The CCSD(T) energies were calculated using the explicitly correlated CCSD(T)-F12b method,[14,15] with the cc-pV*n*Z-F12 (*n* = D, T, Q) series of basis sets for C and N,[17] and the aug-cc-pV*n*Z-PP (*n* = D, T, Q, 5) series of basis sets[18] and small-core relativistic pseudopotentials[19] for the transition metal elements. In the following, combinations of basis sets with the same cardinal number *n* will be referred to simply as aV*n*Z, while the mixed basis of cc-pVQZ-F12 and aug-cc-pV5Z-PP will be denoted aV5Z*. Density fitting (DF) within the correlation treatment used the aug-cc-pV*n*Z(-PP)/MP2Fit[20,21] auxiliary basis sets (ABSs), with the Fock matrix fit using the def2-QZVPP/JKFit[22] ABS for transition metals and cc-pV*n*Z/JKFit[23] sets for lighter elements. The exact combinations of orbital basis sets (OBS) and ABSs are the same as those recommended elsewhere.[24] The CABS approach[25] for the resolution of the identity (RI) employed the compact OptRI ABSs matched to the corresponding OBS.[26,27] A value of 1.4 a_0^{-1} was utilized for the geminal Slater exponent, as this has been shown to provide good results for other transition metal containing systems.[27] As existing basis set extrapolation schemes for F12 methods have not been calibrated for transition metal elements, extrapolation of correlation energies was not carried out in this investigation, but previous experience suggests that the largest basis set combinations of this work should provide results very close to the true complete basis set (CBS) limit. The total electronic energy included the contribution from CABS singles relaxation.[14,28] In the few atomic calculations that were carried out, the CCSD(T)-F12b calculations utilized restricted open-shell Hartree-Fock orbitals but with some spin contamination allowed in the CCSD calculations,[29,30] i.e., R/UCCSD(T)-F12b.

The ΔCV correction was obtained as $E_{\text{core+val}} - E_{\text{val}}$, where $E_{\text{core+val}}$ correlated the 1*s* electrons on C and N, the 3*s*3*p* electrons on Cu, 4*s*4*p* on Ag, and 5*s*5*p* on Au (the 'outer-core' electrons for the transition metal elements). Both of the required energy evaluations were performed at the CCSD(T)-F12b level using the cc-pCVTZ-F12[31] OBS for C and N, and the aug-cc-pwCVTZ-PP OBS for the transition metal elements.[18] DF of the Fock matrix used the same ABSs as in the valence-only calculations, with all other two-electron integral densities fitted with the aug-cc-pwCVTZ(-PP)/MP2Fit[21] ABSs. OptRI ABSs[27,31] were once again employed in the CABS approach, as was a geminal Slater exponent of 1.4 a_0^{-1}.

The ΔDK term provides corrections for two components, firstly the scalar relativistic effects of C and N, and secondly an estimate of errors due to the PP approximation. This term was evaluated as $\Delta\text{DK} = E_{\text{DK}} - E_{\text{PP}}$, where E_{DK} is the total DKH CCSD(T) energy. Two different values were calculated, a frozen-core result using the cc-pVTZ-DK[18,32] basis sets and a correction that used valence and outer-core correlation (as in ΔCV above) with the cc-pwCVTZ-DK[18,32,33] basis sets. For CuCN and AgCN E_{DK} is computed using the second-order DKH Hamiltonian,[16] with third-order DKH[34] and the corresponding DKH3 contracted basis sets for Au employed for AuCN.[18] E_{PP} was computed using cc-pVTZ[35] and cc-pVTZ-PP[18] basis sets in the valence case, where the valence and outer-core calculations employed the cc-pwCVTZ[33] and cc-pwCVTZ-PP[18] sets. Care was taken to ensure the 4*f* orbitals were rotated below the 5*s* and 5*p* orbitals in the AuCN case for these calculations.

For AuCN the Δ4*f* correction was evaluated at the CCSD(T) level as $\Delta 4f = E_{\text{DKH-CV}4f\,5s5p} - E_{\text{DKH-CV}5s5p}$, with a second-order DKH Hamiltonian used throughout. Both sets of calculations correlated the 1*s* electrons on C and N and the 5*s*5*p* orbitals on Au. The $E_{\text{DKH-CV}4f\,5s5p}$ energies also correlated the 4*f* electrons on Au, which required a specific OBS to be developed (denoted cc-pwCVTZ-DK+4*f*) in the same manner as those reported previously for the other 5*d* elements Hf–Pt.[36] These basis sets are based on the cc-pwCVTZ-DK all-electron sets,[18] augmented with additional tight 2*f*2*g*1*h* functions optimized for 4*f* correlation. The resulting exponents and contraction coefficients for this basis set, together with the analogous set for Hg, are included as supporting information.

The cc-pwCVTZ-DK basis set was utilized for all other elements in the calculation of this term.

The effects of higher order electron correlation beyond CCSD(T), ΔHC, were evaluated using high order coupled cluster theory within the frozen core approximation:

$$\Delta HC = \Delta T + \Delta(Q) \qquad (3)$$

ΔT corrects for the effects of iterative triple excitations[30,37] as $\Delta T = E_{CCSDT} - E_{CCSD(T)}$, where both energies were computed using the cc-pVTZ[35] and cc-pVTZ-PP[18] basis sets. The effects of the noniterative quadruple excitations,[38] Δ(Q), is determined by $\Delta(Q) = E_{CCSDT(Q)} - E_{CCSDT}$, using the cc-pVDZ[35] and cc-pVDZ-PP[18] basis sets. As an alternative to Δ(Q), the effects of quadruple excitations were also approximated using the CCSDT(Q)$_\Lambda$ method[39] with a resulting correction $\Delta(Q)_\Lambda = E_{CCSDT(Q)_\Lambda} - E_{CCSDT}$.

In order to determine the effects of molecular spin-orbit (SO) coupling on the PESs, two relativistic CCSD(T) calculations[40] were carried out at each geometry defining the surfaces. The first utilized the molecular-mean-field Hamiltonian approach within the Exact 2-component Dirac-Coulomb Hamiltonian, X2Cmmf-DC-CCSD(T).[41] The second calculation was nearly identical but utilized the spin-free Hamiltonian of Dyall.[42] The total SO effect at each geometry was obtained as the difference in these two energies. In both cases standard uncontracted cc-pVTZ basis sets[35,43] were used for C, N, and Cu while the relativistic cc-pVTZ sets (uncontracted) of Dyall[44] were used for Ag and Au. For the calculation of atomization energies, which required open-shell atomic calculations, the X2Cmmf approach could not be used. In these cases the molecular mean field $^4DC^{**}$ Hamiltonian as described in Ref. 41 was used for both the metal atoms and the required molecular calculations at the equilibrium geometries. Atomic spin-orbit corrections for C and N were derived from their experimental spin-orbit energy levels.[45]

Except for the spin-orbit calculations, which were carried out with the DIRAC program,[46] all other ab initio calculations were performed with the MOLPRO[47] package of ab initio programs and the MRCC[48] program (for high order coupled cluster) interfaced to MOLPRO.

The grids of 50 energies at the various stages of the composite protocol detailed in Eqs. (1) and (2) were fit to polynomial functions of the form:

$$V(Q_1,Q_2,Q_3) = \sum_{ijk} C_{ijk} (Q_1)^i (Q_2)^j (Q_3)^k \qquad (4)$$

Where the coordinates $Q_1 = r_1 - r_{1e}$, , $Q_2 = r_2 - r_{2e}$, and $Q_3 = \theta - \theta_e$. A full set of quartic coefficients were employed, along with diagonal quintic and sextic. The root-mean-square errors of the fits were 0.07, 0.04 and 0.17 cm^{-1} for CuCN, AgCN and AuCN, respectively, with respective maximum errors of 0.24, 0.09 and 0.40 cm^{-1}. The surface fitting and determination of spectroscopic constants *via* second-order perturbation theory[49] was carried out using the SURFIT[50] program. The resulting coefficients from Eq. (4) are provided as supplementary material.[51]

Electric dipole moments were calculated at the same 50 points as the PESs using the CCSD(T) method with the aug-cc-pVTZ basis sets for C and N[35,55] and the aug-cc-pVTZ-PP basis sets and pseudopotentials for the group 11 elements. Finite electric fields of ±0.002 a.u. were applied to the one-electron Hamiltonian, and the resulting *y* and *z* components of the dipoles were separately fit to quartic polynomials of the same form as Eq. (4). The expansion coefficients of the fitted functions are provided in Table SII in the supplementary material. As shown there, the equilibrium dipole moments are all quite large, being -7.21 D for CuCN, -7.70 D for AgCN, and -6.01 D for AuCN with the negative sign indicating the negative end of the dipole is towards N.

Calculations of the ro-vibrational spectra were performed with the EVEREST code,[52] which employed the composite potential energy surfaces described above and 3-dimensional electric dipole moment functions. A similar approach has also recently been used to investigate both the CCN and HS_2 radicals.[53,54] EVEREST uses the exact kinetic energy operator in internal coordinates and a DVR approach. Jacobi coordinates were used, and it was verified that the results fully agree with valence bond-length, bond-angle (BLBA) coordinates. The basis sets utilized for the CN bond and Jacobi angle were 40 Sinc-DVR functions[56] on a 1.85–2.75 bohr interval, and 180 associated Legendre functions, respectively. Forty Sinc-DVR functions were used for the coinage metal to CN center-of-mass distance, built on the 3.8–6.4 bohr interval for CuCN and AgCN, and a 4.2–6.0 bohr interval for AuCN. In all cases, full 3D (without contractions) DVR diagonalization was performed for rotation-free wave functions up to 3000 cm^{-1} (3800 cm^{-1} for CuCN) above the ground vibrational level, and for $\ell = 0 - 6$ (vibrational angular

momentum quantum number). The iterative Jacobi-Davidson algorithm was used for the diagonalization. These vibrational functions were further used to build and diagonalize the full ro-vibrational Hamiltonian for $J = 0 – 3$, and to evaluate vibrational transition dipole moments in the Eckart frame. The transition dipole moments, which were calculated using the partition function-based formula of Ref. 53, were used to simulate vibrational spectra at T = 5 K and T = 300 K.

III. RESULTS AND DISCUSSION

A. The X $^1\Sigma^+$ states

The dependence of the equilibrium bond lengths and harmonic frequencies with respect to basis set size and the various contributions in Eq. (2) are presented in Table I for AuCN. Note that throughout this text, ω_1 corresponds principally to the CN stretch, ω_2 to the bend, and ω_3 to the M-CN stretch. It can be seen in Table I that the convergence of the CCSD(T)-F12b results with respect to basis set size is very rapid; the aVDZ basis provides reasonable results and beyond aVTZ only minimal changes of less than one thousandth of an angstrom and around one wavenumber are observed. The effect of increasing the basis set on Au from aug-cc-pVQZ-PP to aug-cc-pV5Z-PP is practically negligible. Although this suggests that using the aVQZ basis with the F12b method is likely to be sufficient in most cases, the aV5Z* basis is used as the CCSD(T) energy in Eqs. (1) and (2) for the rest of this investigation. Upon comparison with previous conventional CCSD(T) calculations,[5,10] it can be seen that the present results demonstrate significantly longer bond lengths (by 0.0084 Å for Au–C and 0.0016 Å for C–N compared to the cc-pVQZ work of Ref. 5) and correspondingly red-shifted vibrational frequencies (–9.8 cm^{-1} for ω_1, –11.3 cm^{-1} for ω_2, and –9.4 cm^{-1} for ω_3 upon comparison to Ref. 5). This is an indication that the previous investigations did not reach the same level of convergence with respect to the basis set as afforded by explicitly correlated wavefunctions, or that the additional diffuse functions in the current investigation had a larger effect than might have been anticipated.

The effect of correlating the 1s electrons on C and N and the outer core electrons on Au contracts the Au–C and C–N bond lengths by 0.0086 and 0.0025 Å, respectively. It

also blue shifts the harmonic frequencies by 9.3, 6.9 and 9.0 cm^{-1}. This effect is roughly equivalent to that observed previously at the CCSD(T)/cc-pVQZ level.[5] A comparison of correlating only the valence electrons in the ΔDK correction (Val in Table I) and correlating valence and outer-core (Val + CV in Table I) indicates that while this correction is small in magnitude, these two choices can lead to contributions of opposite sign. For example, correlating only the valence electrons reduces the Au–C bond length by –0.0018 Å, yet correlating both the valence and outer core increases the bond length by 0.0014 Å. Overall the effect of the ΔDK correction is small, especially when both the valence and outer core are correlated, and the latter choice will be employed in the composite scheme herein.

The Au 4*f* electrons are typically replaced by the PP, yet their correlation can lead to non-negligible effects in some properties of 5*d* transition metal elements.[36] The results of the Δ4*f* correction for AuCN in Table I show that the biggest effect is on the Au–C bond length, which is contracted by 0.0041 Å. The effect on the vibrational frequencies reaches a maximum of +2.6 cm^{-1} for ω_3, indicating that when high accuracy is the goal, 4*f* correlation should be accounted for. In terms of the higher order correlation corrections, ΔHC, it can be seen that the ΔT and Δ(Q) components move the bond lengths and harmonic frequencies in opposite directions. The overall effect is to increase the Au–C and C–N bond lengths by 0.0017 and 0.0009 Å, respectively, and red shift the frequencies by –10.1, –1.6 and –1.4 cm^{-1}. The differences between the (Q) and $(Q)_\Lambda$ bond lengths and harmonic frequencies are small, with the largest difference being a 2.2 cm^{-1} change in ω_1. The precision of the experimental results currently available is not sufficient to establish which of these approaches produces the more accurate results, but CCSDT(Q) was chosen for the production of the PESs simply because it is more commonly used. Whilst checking the convergence with respect to even higher order correlation or using larger basis sets than cc-pVDZ(-PP) for Δ(Q) is desirable, the steep scaling (recalling that each PES requires 50 points) of these methods ensures that such calculations are beyond the computational resources available at the time of this investigation.

The inclusion of molecular SO effects reduces the Au–C bond length by 0.0028 Å, but they have a smaller influence on the remaining properties in Table I, increasing the

C–N bond length by a negligible 0.0001 Å, decreasing ω_1 by 0.9 cm^{-1}, and increasing ω_2 and ω_3 by 1.0 and 3.0 cm^{-1}, respectively. On the whole, as expected for this closed shell molecule, the SO effects are small compared to the majority of the other corrections to the composite energy, but are essential for an accurate description of the bond lengths and vibrational frequencies. The change in bond lengths obtained from these coupled cluster SO calculations is of the same order as those observed previously at the DFT zeroth-order relativistic approximation (ZORA) level.[5] The experimental gas-phase data is derived from rotational spectroscopy and due to the indirect nature in which vibrational data is produced from such studies, the harmonic vibrational frequencies should be treated as rough estimates. Still, agreement between the best theoretical results from Table I and experimental data is good, especially for ω_3, where the difference is only 5.2 cm^{-1}. The experimental bond lengths reported in Table I correspond to a $r_m^{(2)}$ structure and hence are not directly comparable to the calculated r_e values. Nevertheless, the agreement between experiment and theory is reasonably good at around 0.005 Å. A more detailed comparison of molecular structures can be found below.

Convergence data analogous to Table I for CuCN and AgCN are detailed in Tables II and III, respectively, where it can be seen that, given a few small differences, generally the trends are the same. One notable exception are the SO effects, which are essentially negligible for both CuCN and AgCN. The significant effects of scalar relativity can be observed by comparing the bond lengths and harmonic frequencies of the three species. As detailed previously by Schwerdtfeger et al.[11] for several Au(I) molecules, relativity leads to a shortening of the metal-ligand bond length and this is clearly observed in the present case where the M-C distance in AuCN is intermediate in length between that of CuCN and AgCN. Also in agreement with Ref. 11, the stretching force constants are even more sensitive to this relativistic bond contraction, whereby the M-C stretching frequency for AuCN is larger than in AgCN and CuCN by 89 and 7 cm^{-1}, respectively. As noted above, the equilibrium dipole moment of AuCN is more than 1 D smaller in magnitude then either CuCN or AgCN. This is also consistent with an increased negative charge at the Au atom due to the relativistic enhancement of its electronegativity.[11]

Spectroscopic constants from second-order vibrational perturbation theory based on the final composite PESs for CuCN, AgCN and AuCN are given in Table IV. Comparison with previous theoretical work indicates that the M–C bond distance is much more sensitive to level of theory than r(C–N); the CCSD(T)/cc-pVQZ + SO results of Zaleski-Ejgierd agree with the present C–N bond lengths to within 0.0008 Å. while the M-C bond distances only agree to around 0.0060 Å, although this is improved to 0.0029 Å in the case of Cu–C. The experimental values of B_0 are also given in Table IV for CuCN,[6] AgCN[7] and AuCN.[7] The theoretical results in Table IV agree to within 6.2, 1.5 and 4.9 MHz, respectively, representing very good agreement. Likewise the ab initio values for the vibration-rotation interaction constants are in excellent agreement with those values available from experimental work, agreeing to within about 1 MHz in all cases. The trend of the M–CN stretching vibrational frequencies (ω_3) matches those from experimental data, with Ag < Cu < Au, although a quantitative comparison is difficult due to the approximate nature of the vibrational frequencies obtained from rotational spectroscopy experiments and the large error bars for the frequencies determined from photoelectron experiments.[3,8]

For both CuCN and AgCN a strong Fermi resonance is predicted between $2\omega_2$ (bend) and ω_3 (M-C stretch), with the strength of the interaction slightly decreasing from Cu to Ag. This resonance strongly affects the calculated values of the X_{22}, X_{23}, and X_{ll} anharmonicity constants, which is easily observed by comparison with the analogous AuCN values in Table IV. Of course the resulting anharmonic frequencies computed with these anharmonicities are also significantly affected. While this resonance is naturally accounted for in the variational calculations discussed below, Table IV also shows results obtained by employing the deperturbation procedure of Allen et al. [57] This involved factoring the perturbation theory equations for the anharmonicity constants and deleting those terms that involve the $(2\omega_2-\omega_3)$ resonant denominators. The resulting deperturbed values are also shown in Table IV. The fundamental frequencies can then be obtained by diagonalization of the matrix[58]

$$\begin{bmatrix} E(001) & K_{223}/\sqrt{2} \\ K_{223}/\sqrt{2} & E(020) \end{bmatrix} \tag{5}$$

where $E(001)$ and $E(020)$ are the deperturbed energy levels calculated from the deperturbed anharmonicity constants and the Fermi resonance constant $K_{223} = -\phi_{223}/2$, where ϕ_{223} is the cubic force constant in normal coordinates (K_{223} = 48.82 cm^{-1} and 44.06 cm^{-1} for CuCN and AgCN, respectively). The final eigenstates are strongly mixed, 55%:45% in CuCN and 69%:31% in AgCN, but the resulting eigenvalues are now in excellent agreement with the variational results discussed below.

B. Variational calculation of the ro-vibrational spectra

Selected vibrational band origins, together with their calculated integrated intensities, are shown in Table V. A larger set of vibrational levels are given in Table SIV of the Supplemental Information. Upon comparing to the fundamental frequencies of Table IV calculated via vibrational perturbation theory, the variational results agree to better than 1 cm^{-1}. Of course of particular interest is the Fermi resonance interaction between the first overtone of the bend, (02^00), with the M-C stretching mode, (00^01), for M = Cu and Ag. Comparison of the variationally calculated band origins and the eigenvalues of Eq. (5) also agree to within 1 cm^{-1}. The assignment of these bands was difficult due to the heavy mixing of the vibrational wavefunctions. The vibrational wavefunctions for these two modes are shown in Figure 1 for all three molecules as a function of the bending angle θ and the M-C distance (labelled R_2 in these figures). The curvatures of these wavefunctions closely follow those of the PESs, which are shown in Figure 2. Clearly noticeable is how the wavefunctions evolve from CuCN to AuCN, where in the latter case the wavefunctions are nearly pure bending and stretching. The assignments for CuCN and AgCN were facilitated by inspecting the wavefunctions in the R_1, R_2 plane where the bending mode should be nodeless but also by the perturbation analysis via Eq. (5) above. Related to this strong Fermi resonance in CuCN and AgCN, as well as the lack of it in AuCN, is the magnitude of the ℓ-type vibrational anharmonicity in the (020) band. As seen in Table SIV, the (02^00) level lies above the (02^20) by about 40 cm^{-1} in CuCN, by about 20 cm^{-1} in AgCN, and less than 10 cm^{-1} in AuCN. Similar trends are observed in the higher bending overtones, as well as the stretch-bend combination bands with $v_2 > 1$.

In all three molecules the most intense vibrational band is calculated to be the metal-C stretching fundamental, ($00^0$1), which lies between 370 and 470 cm^{-1}. In all three molecules the CN stretching fundamental near 2165 cm^{-1} also carries significant intensity. In regards to the bending modes, the fundamental band is fairly intense in all three cases, and due to the Fermi interaction with the intense ($00^0$1) fundamental (CuCN and AgCN), the first overtone of the bending mode is also relatively intense - even slightly more than its fundamental in the case of AgCN. In regards to the combination bands, the ($11^1$0) carries some intensity but in general those are weak due to relatively small anharmonic couplings. Due to the low-lying bending mode, hot bands associated with this level are predicted to have significant intensity at 300 K, particularly the ($01^1$1) $\leftarrow$ ($01^1$0) band that lies near the ($00^0$1) fundamental. Together with the hot bands arising from the first overtone of the bend, this leads to a complicated band structure at and below 500 cm^{-1} as shown in the simulated vibrational spectra at temperatures of 5 and 300 K in Figure 3, particularly for CuCN and AgCN.

In order to obtain vibration-rotation interaction constants that could be compared to the perturbation theory results of Table IV, rotational constants were calculated from the variational ro-vibrational energies in a few cases. These involved additional calculations for J=0–3 in a vibrational basis that included states up to 7000 cm^{-1} in order to obtained converged results for the ($10^0$0) state. The results are shown in Table VI and compared to the available experimental values. For the most part the agreement with experiment is excellent for the rotational constants, within 6 MHz in all cases, just as in the perturbation theory results of Table IV. In particular the ground state rotational constants from the variational calculations agree with the perturbation theory results to within 0.3 MHz. The variationally calculated value for B($00^0$1), however, is strongly affected by the Fermi resonance of this level with the bending overtone as discussed above, which yields a ($00^0$1) rotational constant *larger* than the ground state value. In the case of AgCN, the rotational constant in v_3=1 was obtained from the microwave spectroscopy experiments of Okabayashi et al.,[7] and as shown in Table VI it is smaller than the ground state value as is typically the case for a stretching fundamental. This yields a B_0–B_v value that is in good agreement with the value of α_3 obtained from vibrational perturbation theory (Table IV). The reason for the poor comparison with the

variationally calculated result is presumably due to the present calculations being restricted to very low values of J, i.e., J=0 – 3, while the experimental work observed transitions involving J from 29 to 49 where evidently the Fermi resonance is no longer very active.

In order to further examine the accuracy of the equilibrium structures produced by the composite method, semi-experimental equilibrium geometries (r_e^{SE}) were calculated by combining the ab initio rotation-vibration interaction constants (α_i) of Table IV with experimental values[59] of the ground state rotational constants B_0 via the Kraitchman equations.[60] The resulting bond distances are shown in Table VII, along with some of the experimental effective structures (r_0, r_s, and $r_m^{(2)}$) and the purely theoretical equilibrium values produced in this investigation (r_e). Excellent agreement is observed between r_e and r_e^{SE} C–N bond distances, with the largest deviation being just 0.0003 Å. The agreement for the M–C bond distances is still very good, but nearly an order of magnitude greater deviations, 0.001 to 0.0023 Å. While it is well known that reaching high accuracy is considerably more difficult for transition metals than lighter elements, Table I suggests that the bond distances are well converged with respect to basis set at the CCSD(T)-F12b level. A likely source of error in the current ab initio values could be found in the higher order electron correlation terms, as the ΔT and Δ(Q) components lengthen and contract the Au-C bond distance by +0.0026 and -0.0009 Å, respectively. It is possible that even higher level electron correlation, e.g., CCSDTQP, may increase agreement with the semi-experimental data, or particularly that larger basis sets for the ΔT and Δ(Q) corrections may also have an effect. However, increasing the correlation level or basis set(s) is currently out of reach for this MCN series of molecules.

C. Thermochemistry

Atomization energies for the $X^1\Sigma^+$ states of the coinage metal cyanides were computed from the composite potentials using Eqs. 1 and 2, where now the ΔSO term also included atomic SO contributions. All of the individual contributions entering into the ΣD_e values are shown in Table VIII. Including the zero-point corrections obtained from the final composite potential energy surfaces (Table SIV) produces ΣD_0 values of

273.08, 261.84, and 265.45 (all in kcal mol^{-1}). Enthalpies of formation at 0 K, ΔH_f(0 K), were then calculated using reference ΔH_f(0 K) values for the atoms (170.024 kcal mol^{-1} for C,[61] 112.469 kcal mol^{-1} for N,[61] 80.36 kcal mol^{-1} for Cu,[62] 67.98 kcal mol^{-1} for Ag,[62] and 87.46 kcal mol^{-1} for Au[63]). The resulting ΔH_f(0 K) values are 89.8 kcal mol^{-1}, 88.6 kcal mol^{-1}, and 104.5 kcal mol^{-1} for CuCN, AgCN, and AuCN, respectively. Based primarily on the results for the higher order correlation contributions, where the ΔT and Δ(Q) contributions are opposite in sign and Δ(Q) and $\Delta(Q)_\Lambda$ have comparable magnitudes, these molecules appear well-behaved in regards to the present composite methodology. Hence the final predicted atomization energies and formation enthalpies are expected to be accurate to at least 1 kcal mol^{-1}.

IV. CONCLUSIONS

In the present work accurate near-equilibrium potential energy and dipole moment surfaces have been calculated for the closed-shell, linear, coinage-metal cyanides. The PESs were determined using a composite approach utilizing the explicitly correlated CCSD(T)-F12b method with corrections for core correlation, molecular spin-orbit coupling, scalar relativity, and electron correlation beyond CCSD(T). Ro-vibrational spectroscopic properties have been calculated from the fitted PESs using both 2nd-order vibrational perturbation theory and variational methods. Where available the agreement with experiment is excellent and numerous predictions have been made, especially for the ro-vibrational spectra. In particular a strong Fermi resonance between the first overtone of the bending mode and the fundamental of the metal-C stretch is predicted for both CuCN and AgCN. Semi-experimental equilibrium structures are also reported that utilize the ab initio vibration-rotation interaction constants and the accurate experimental ground state rotational constants. The same composite approach has been used to determine accurate enthalpies of formation for each species.

ACKNOWLEDGMENTS

J.G.H. is grateful to the Royal Society of Edinburgh and Scottish Government for a personal research fellowship. K.A.P. acknowledges the support of the U.S. DOE

BES/HEC through grant DE-FG02-12ER16329. The authors are particularly indebted to the critical reading of the manuscript by the referees. The authors would like to thank Prof. Pekka Pyykkö for bringing these interesting molecules to our attention. K.A.P. thanks Dr. Stefan Knecht for his help with the spin-orbit calculations.

REFERENCES

[1] S. H. Bertz and E. H. Fairchild, in *Encyclopedia of Reagents for Organic Synthesis*, edited by L. Paquette (Wiley, New York, 1995), pp. 1341.

[2] J. Gómez-Díaz, K. Honkala, and N. López, Surf. Sci. **604**, 1552 (2010).

[3] X. Wu, Z. Qin, H. Xie, R. Cong, X. Wu, Z. Tang, and H. Fan, J. Phys. Chem. A **114**, 12839 (2010).

[4] O. Dietz, V. Rayon, and G. Frenking, Inorg. Chem. **42**, 4977 (2003); A. Veldkamp and G. Frenking, Organomet. **12**, 4613 (1993).

[5] P. Zaleski-Ejgierd, M. Patzschke, and P. Pyykkö, J. Chem. Phys. **128**, 224303 (2008).

[6] D. B. Grotjahn, M. Brewster, and L. M. Ziurys, J. Am. Chem. Soc. **124**, 5895 (2002).

[7] T. Okabayashi, E. Y. Okabayashi, F. Koto, T. Ishida, and M. Tanimoto, J. Am. Chem. Soc. **131**, 11712 (2009).

[8] A. Boldyrev, X. Li, and L. Wang, J. Chem. Phys. **112**, 3627 (2000).

[9] A. Paul, Y. Yamaguchi, and H. F. Schaefer, J. Chem. Phys. **127**, 154324 (2007).

[10] P. Schwerdtfeger and M. Lein, in *Gold Chemistry*, edited by F. Mohr (Wiley, Weinheim, 2009), pp. 183.

[11] P. Schwerdtfeger, P. D. W. Boyd, A. K. Burrell, W. T. Robinson, and M. J. Taylor, Inorg. Chem. **29**, 3593 (1990).

[12] D.-K. Lee, I. S. Lim, Y. S. Lee, D. Hagebaum-Reignier, and G.-H. Jeung, J. Chem. Phys. **126**, 244313 (2007); J. Seminario, A. Zacarias, and J. Tour, J. Am. Chem. Soc. **121**, 411 (1999).

[13] H.-J. Werner, T. B. Adler, G. Knizia, and F. R. Manby, in *Recent Progress in Coupled Cluster Methods: Theory and Applications*, edited by P. Čársky, J. Paldus, and J. Pittner (Springer, Berlin, 2010), pp. 573; D. Tew, C. Hättig, R. Bachorz, and W.

Klopper, in *Recent Progress in Coupled Cluster Methods: Theory and Applications*, edited by P. Čársky, J. Paldus, and J. Pittner (Springer, Berlin, 2010), pp. 535.

[14] T. B. Adler, G. Knizia, and H.-J. Werner, J. Chem. Phys. **127**, 221106 (2007).

[15] G. Knizia, T. B. Adler, and H.-J. Werner, J. Chem. Phys. **130**, 054104 (2009).

[16] M. Douglas and N. M. Kroll, Ann. Phys. (N.Y.) **82**, 89 (1974); G. Jansen and B. A. Hess, Phys. Rev. A **39**, 6016 (1989).

[17] K. A. Peterson, T. B. Adler, and H.-J. Werner, J. Chem. Phys. **128**, 084102 (2008).

[18] K. A. Peterson and C. Puzzarini, Theor. Chem. Acc. **114**, 283 (2005).

[19] D. Figgen, G. Rauhut, M. Dolg, and H. Stoll, Chem. Phys. **311**, 227 (2005).

[20] F. Weigend, A. Köhn, and C. Hättig, J. Chem. Phys. **116**, 3175 (2002).

[21] C. Hättig, Phys. Chem. Chem. Phys. **7**, 59 (2005); C. Hättig, Unpublished results, available from the Turbomole library.

[22] F. Weigend, J. Comput. Chem. **29**, 167 (2008).

[23] F. Weigend, Phys. Chem. Chem. Phys. **4**, 4285 (2002).

[24] J. G. Hill, K. A. Peterson, G. Knizia, and H.-J. Werner, J. Chem. Phys. **131**, 194105 (2009).

[25] E. F. Valeev, Chem. Phys. Lett. **395**, 190 (2004).

[26] K. E. Yousaf and K. A. Peterson, J. Chem. Phys. **129**, 184108 (2008); K. E. Yousaf and K. A. Peterson, Chem. Phys. Lett. **476**, 303 (2009).

[27] J. G. Hill and K. A. Peterson, J Chem Theory Comput **8**, 518 (2012).

[28] G. Knizia and H.-J. Werner, J. Chem. Phys. **128**, 154103 (2008).

[29] P. J. Knowles, C. Hampel, and H.-J. Werner, J. Chem. Phys. **99**, 5219 (1993).

[30] G. E. Scuseria and H. F. Schaefer, Chem. Phys. Lett. **152**, 382 (1988).

[31] J. G. Hill, S. Mazumder, and K. A. Peterson, J. Chem. Phys. **132**, 054108 (2010).

[32] W. de Jong, R. Harrison, and D. Dixon, J. Chem. Phys. **114**, 48 (2001).

[33] K. A. Peterson and T. Dunning Jr, J. Chem. Phys. **117**, 10548 (2002).

[34] M. Reiher and A. Wolf, J. Chem. Phys. **121**, 2037 (2004); M. Reiher and A. Wolf, J. Chem. Phys. **121**, 10945 (2004).

[35] T. H. Dunning Jr, J. Chem. Phys. **90**, 1007 (1989).

[36] D. Figgen, K. A. Peterson, M. Dolg, and H. Stoll, J. Chem. Phys. **130**, 164108 (2009).

[37] J. Noga and R. J. Bartlett, J. Chem. Phys. **86**, 7041 (1987).

[38] Y. J. Bomble, J. F. Stanton, M. Kallay, and J. Gauss, J. Chem. Phys. **123**, 054101 (2005).

[39] M. Kallay and J. Gauss, J. Chem. Phys. **123**, 214105 (2005).

[40] L. Visscher, T. J. Lee, and K. Dyall, J. Chem. Phys. **105**, 8769 (1996).

[41] J. Sikkema, L. Visscher, T. Saue, and M. Ilias, J. Chem. Phys. **131**, 124116 (2009).

[42] K. Dyall, J. Chem. Phys. **100**, 2118 (1994).

[43] N. B. Balabanov and K. A. Peterson, J. Chem. Phys. **123**, 064107 (2005).

[44] K. Dyall, Theor. Chem. Acc. **112**, 403 (2004); K. Dyall, Theor. Chem. Acc. **117**, 483 (2007).

[45] C. E. Moore, *Atomic Energy Levels*. (NSRDS-NBS 35; Office of Standard Reference Data, National Bureau of Standards, Washington DC, 1971).

[46] DIRAC, a relativistic ab initio electronic structure program, Release DIRAC11 (2011), written by R. Bast, H. J. Aa. Jensen, T. Saue, and L. Visscher, with contributions from V. Bakken, K. G. Dyall, S. Dubillard, U. Ekström, E. Eliav, T. Enevoldsen, T. Fleig, O. Fossgaard, A. S. P. Gomes, T. Helgaker, J. K. Lærdahl, J. Henriksson, M. Iliaš, Ch. R. Jacob, S. Knecht, C. V. Larsen, H. S. Nataraj, P. Norman, G. Olejniczak, J. Olsen, J. K. Pedersen, M. Pernpointner, K. Ruud, P. Sałek, B. Schimmelpfennig, J. Sikkema, A. J. Thorvaldsen, J. Thyssen, J. van Stralen, S. Villaume, O. Visser, T. Winther, and S. Yamamoto (see http://dirac.chem.vu.nl).

[47] MOLPRO, version 2010.1, a package of ab initio programs, H.-J. Werner, P. J. Knowles, G. Knizia, F. R. Manby, M. Schütz and others, see http://www.molpro.net; H.-J. Werner, P. J. Knowles, G. Knizia, F. R. Manby, and M. Schütz, WIREs Comput Mol Sci **00**, 1 (2011).

[48] MRCC, a string-based quantum chemical program suite, Budapest University of Technology and Economics, 2001; M. Kállay and P. R. Surján, J. Chem. Phys. **115**, 2945 (2001).

[49] A. R. Hoy, I. M. Mills, and G. Strey, Mol. Phys. **24**, 1265 (1972); I. M. Mills, in *Molecular Spectroscopy: Modern Research*, edited by K. N. Rao and C. W. Mathews (Academic, New York, 1972), Vol. 1.

[50] J. Senekowitsch, Ph.D. thesis, Universität Frankfurt, Frankfurt, Germany, 1988.

[51] See Supplementary Material Document No._____ for Tables SI-SIII and the cc-pwCVTZ-DK+4f basis sets. For information on Supplementary Material, see http://www.aip.org/pubservs/epaps.html.

[52] A. O. Mitrushchenkov, J. Chem. Phys. **136**, 024108 (2012).

[53] J. G. Hill, A. O. Mitrushchenkov, K. E. Yousaf, and K. A. Peterson, J. Chem. Phys. **135**, 144309 (2011).

[54] K. A. Peterson, A. O. Mitrushchenkov, and J. S. Francisco, Chem. Phys. **346**, 34 (2008).

[55] R. A. Kendall, T. H. Dunning Jr, and R. J. Harrison, J. Chem. Phys. **96**, 6796 (1992).

[56] D. T. Colbert and W. H. Miller, J. Chem. Phys. **96**, 1982 (1991).

[57] W. D. Allen, Y. Yamaguchi, A. G. Csaszar, D. A. Clabo Jr., R. B. Remington, and H. F. Schaefer III, Chem. Phys. **145**, 427 (1990).

[58] G. Amat and M. Pimbert, J. Mol. Spectrosc. **16**, 278 (1965); D. M. Papousek and M. R. Aliev, *Molecular Rotation-Vibration Spectra*. (North-Holland, Amsterdam, 1982).

[59] M. D. Harmony, in *Vibrational Spectra and Structure* (Elsevier, 1999), Vol. 24, pp. 1.

[60] J. Kraitchman, Am. J. Phys. **21**, 17 (1953).

[61] W. R. Stevens, B. Ruscic, and T. Baer, J. Phys. Chem. A **114**, 13134 (2010).

[62] J. D. Cox, D. D. Wagman, and V. A. Medvedev, *CODATA Key Values for Thermodynamics*. (Hemisphere Publishing Corp., New York, 1989).

[63] D. D. Wagman, W. H. Evans, V. B. Parker, R. H. Schumm, I. Halow, S. M. Bailey, K. L. Churney, and R. L. Nuttall, J. Phys. Chem. Ref. Data **11**, Supplement 2 (1982).

[64] J. Senekowitsch, S. Carter, A. Zilch, H.-J. Werner, N. C. Handy, and P. Rosmus, J. Chem. Phys. **90**, 783 (1989).

TABLE I. Convergence of the CCSD(T)-F12b calculated $X^1\Sigma^+$ AuCN equilibrium bond lengths (Å) and harmonic vibrational frequencies (ω_i in cm^{-1}) with respect to basis set as well as other contributions detailed in Eq. (2). See text for further details.

	r_{Au-C}	r_{C-N}	ω_1	ω_2	ω_3
aVDZ	1.9235	1.1637	2207.4	274.3	467.6
aVTZ	1.9204	1.1640	2205.4	276.5	471.7
aVQZ	1.9196	1.1639	2205.7	277.9	472.8
aV5Z*	1.9196	1.1639	2205.6	277.6	472.9
ΔCV	−0.0086	−0.0025	+9.3	+6.9	+9.0
Δ4*f*	−0.0041	0.0000	+0.4	+1.4	+2.6
ΔDK					
Val	−0.0018	−0.0003	−0.5	+3.2	+2.1
Val+CV	+0.0014	−0.0002	−0.6	−1.4	−0.9
ΔT	+0.0026	−0.0010	+10.8	+0.3	−1.7
Δ(Q)	−0.0009	+0.0019	−20.9	−1.9	+0.2
$\Delta(Q)_\Lambda$	−0.0010	+0.0017	−18.7	−1.7	+0.3
ΔSO	−0.0028	+0.0001	−0.9	+1.0	+3.0
Final composite	1.9071	1.1623	2203.8	284.1	485.2
Expt. [a]	1.9123	1.1587	---	320	480 502(10)[b]

[a] From the microwave experiments of Ref. 7. The bond lengths correspond to a r_s (substitution) structure. See also Table V.

[b] Photoelectron imaging result of Ref. 3.

TABLE II. Convergence of the CCSD(T)-F12b calculated $X^1\Sigma^+$ CuCN equilibrium bond lengths (Å) and harmonic vibrational frequencies (ω_i in cm^{-1}) with respect to basis set as well as other contributions detailed in Eq. (2). See text for further details.

	r_{Cu-C}	r_{C-N}	ω_1	ω_2	ω_3
aVDZ	1.8257	1.1654	2195.4	242.2	474.6
aVTZ	1.8238	1.1657	2193.6	242.8	476.6
aVQZ	1.8233	1.1656	2193.7	243.9	477.9
aV5Z*	1.8234	1.1656	2193.6	243.5	477.8
ΔCV	−0.0004	−0.0026	+10.0	+2.8	+1.0
ΔDK					
Val	+0.0019	−0.0003	+0.1	+0.9	0.0
Val+CV	+0.0023	−0.0002	−0.3	+0.3	−0.1
ΔT	+0.0026	−0.0009	+10.2	+0.3	−0.5
Δ(Q)	−0.0014	+0.0018	−21.1	−1.0	+0.2
$\Delta(Q)_\Lambda$	−0.0016	+0.0017	−19.1	−1.0	−0.2
ΔSO	−0.0001	0.0000	−0.1	+0.1	+0.1
Final composite	1.8265	1.1637	2192.4	246.0	478.4
Expt.[a]	1.8296	1.1621	---	270	478 480(30)[b] 460(50)[c]

[a] From the microwave experiments of Ref. 6. The bond lengths correspond to a $r_m^{(2)}$ structure. See also Table V.

[b] From the photoelectron experiments of Ref. 8.

[c] Photoelectron imaging results of Ref. 3.

TABLE III. Convergence of the CCSD(T)-F12b calculated $X^1\Sigma^+$ AgCN equilibrium bond lengths (Å) and harmonic vibrational frequencies (ω_i in cm^{-1}) with respect to basis set as well as other contributions detailed in Eq. (2). See text for further details.

	r_{Ag-C}	r_{C-N}	ω_1	ω_2	ω_3
aVDZ	2.0398	1.1650	2193.7	205.9	389.9
aVTZ	2.0352	1.1652	2191.9	208.0	392.2
aVQZ	2.0339	1.1651	2192.0	209.5	393.4
aV5Z*	2.0341	1.1651	2191.8	208.3	393.0
ΔCV	−0.0124	−0.0027	+10.4	+6.8	+7.2
ΔDK					
Val	+0.0028	−0.0004	+0.5	+0.1	+0.3
Val+CV	+0.0070	−0.0001	−1.1	−1.4	−3.3
ΔT	+0.0024	−0.0008	+8.9	+0.1	−1.0
Δ(Q)	−0.0009	+0.0016	−18.5	−1.3	−0.2
$\Delta(Q)_\Lambda$	−0.0010	+0.0015	−16.9	−1.2	+0.5
ΔSO	−0.0004	0.0000	0.0	+0.2	+0.2
Final total	2.0299	1.1632	2191.6	212.7	396.0
Expt. [a]	2.0312	1.1603	---	240	400 390(30)[b] 385(27)[c]

[a] From the microwave experiments of Ref. 7. The bond lengths correspond to a $r_m^{(2)}$ structure. See also Table V.

[b] From the photoelectron experiments of Ref. 8.

[c] Photoelectron imaging results of Ref. 3.

TABLE IV. Spectroscopic constants of CuCN, AgCN and AuCN derived from the final composite PESs using second-order vibrational perturbation theory. All values were calculated for the most abundant isotopomers.[a]

Constant	CuCN	AgCN	AuCN
r_e (M–C) (Å)	1.8265	2.0299	1.9071
r_e (C–N) (Å)	1.1637	1.1632	1.1623
B_e (MHz)	4229.8	3233.1	3237.5
B_0 (MHz)	4231.2	3236.1	3235.1
	[4224.9768][b]	[3237.5618][b]	[3230.2112][b]
α_1 (MHz)	20.00	14.51	14.55
α_2 (MHz)	-21.07	-17.07	-10.98
	[-22.1244][b]	[-17.6538][b]	[-11.9781][b]
α_3 (MHz)	19.37	13.69	12.17
		[14.2859][b]	
D_e (kHz)	1.40	0.92	0.62
q_e (MHz)	5.45	3.62	2.80
ω_1 (cm^{-1})	2192.4	2191.6	2203.8
ω_2 (cm^{-1})	246.0	212.7	284.1
ω_3 (cm^{-1})	478.4	396.0	485.2
X_{11} (cm^{-1})	-12.33	-12.42	-12.52
X_{12} (cm^{-1})	-4.15	-3.84	-5.42
X_{13} (cm^{-1})	-0.75	-0.84	-1.36
X_{22} (cm^{-1})	21.26[c]	7.89[c]	2.19
	(-0.81)	(-0.37)	
X_{23} (cm^{-1})	-91.15[c]	-35.25[c]	-11.51
	(-2.86)	(-2.21)	
X_{33} (cm^{-1})	-1.93	-1.41	-1.72
X_{ll} (cm^{-1})	-21.96[c]	-8.26[c]	-2.19
	(0.11)	(0.00)	
v_1 (cm^{-1})	2163.2	2162.5	2172.7
v_2 (cm^{-1})	240.3	208.6	280.1

ν_3 (cm^{-1})	383.0 [c]	357.5 [c]	469.5
	(440.1)	(369.7)	

[a] Note that the labels of the vibrational modes predominately correspond to 1 = CN stretch, 2 = bend, 3 = MC stretch.

[b] Experimental values from the microwave spectroscopy experiments of Grotjahn et al.[6] (CuCN) and Okabayashi et al.[7] (AgCN and AuCN). The experimental α_i values were estimated from the experimental B_0–B_v differences.

[c] Perturbed by a $2\omega_2 : \omega_3$ Fermi resonance. The X_{ij} values here in parentheses correspond to deperturbed values using the scheme of Ref. 57. The fundamental frequencies here in parentheses have been calculated via diagonalization of a 2×2 Fermi resonance matrix using the deperturbed energy levels and calculated Fermi resonance constants. See the text.

Table V. Selected fundamental, overtone, combination, and hot band origins (in cm^{-1}) determined in variational nuclear motion calculations together with their integrated absorption intensities (in cm^{-2} atm^{-1} at 300 K).[a]

	CuCN		AgCN		AuCN	
Band	Freq.	Intensity	Freq.	Intensity	Freq.	Intensity
$(01^10) \leftarrow (00^00)$	240.61	8.32	208.61	3.88	280.50	2.27
(00^01)	440.97	15.20	370.34	14.10	469.89	8.16
(02^00)	509.93	7.57	436.12	5.27	570.00	0.13×10^{-3}
(01^11)	664.87	0.30×10^{-2}	565.18	0.22×10^{-2}	740.51	0.11×10^{-2}
(00^02)	864.18	0.49×10^{-2}	729.85	0.011	935.39	0.18×10^{-3}
(10^00)	2163.09	5.27	2162.38	4.42	2172.39	4.51
(11^10)	2399.60	0.44	2367.15	0.29	2447.45	0.81
$(02^20) \leftarrow (01^10)$	239.82	5.26	208.11	2.87	280.97	1.19
(01^11)	424.26	10.20	356.57	9.88	460.00	4.72
(03^10)	521.77	4.54	445.92	4.42	578.51	0.28×10^{-2}
(11^10)	2158.99	3.42	2158.54	3.29	2166.95	2.49
(12^20)	2394.73	0.27	2362.80	0.21	2442.47	0.41
$(03^30) \leftarrow (02^20)$	239.17	2.51	207.64	1.60	281.47	0.47
(02^21)	411.06	3.39	345.45	3.59	450.91	1.34
(13^30)	2390.02	0.12	2358.46	0.11	2437.53	0.15
$(01^12) \leftarrow (01^11)$	410.82	2.46	347.78	3.21	455.42	1.05
$(00^02) \leftarrow (00^01)$	423.20	3.18	359.51	4.01	465.49	1.73

[a] The theoretical values correspond to pure vibrational transition energies without rotation. The integrated intensities were calculated using the Eckart frame, pure vibrational dipole moment expression (see Ref. 64). The calculated zero-point levels are given in Table SIV in the Supplemental Information.

Table VI. Rotational constants (MHz) calculated from the variational ro-vibrational energy levels. Experimental values[a] are given in square brackets while results using perturbation theory are given in parentheses.

	CuCN		AgCN		AuCN	
State	B_v	$B_0 - B_v$	B_v	$B_0 - B_v$	B_v	$B_0 - B_v$
(00^00)	4231.4		3236.0		3235.4	
	(4231.2)		(3236.1)		(3235.1)	
	[4224.977]		[3237.562]		[3230.211]	
(10^00)	4211.9	19.5	3221.7	14.3	3221.3	14.1
		(20.0)		(14.5)		(14.6)
(00^01)	4247.5 [b]	-16.1 [b]	3242.5 [b]	-6.5 [b]	3228.7	6.7
		(19.4)		(13.7)		(12.2)
			[3223.276]	[14.286]		
(01^10)	4253.4	-22.0	3253.5	-17.5	3247.2	-11.8
		(-21.1)		(-17.1)		(-11.0)
	[4247.101]	[-22.12]	[3255.216]	[-17.65]	[3242.189]	[-11.98]
(02^00)	4240.5	-9.1	3254.1	-18.1		
(02^20)	4276.0	-44.6	3259.3	-23.3		
	[4269.642]	[-44.66]				

[a] Ref. 6 for CuCN and Ref. 7 for AgCN and AuCN.

[b] The (00^01) and (02^00) are strongly mixed via Fermi resonance including J=0-3 from which these rotational constants were derived. See the text.

TABLE VII. Molecular structures (in Å) of CuCN, AgCN and AuCN.

Molecule	Structure type	r (M–C)	r (C–N)
CuCN	r_0 [a]	1.8323	1.1576
	$r_m^{(2)}$	1.8296	1.1621
	r_e (this work)[c]	1.8265	1.1637
	r_e^{SE} (this work)[d]	1.8287	1.1636
AgCN	r_0 [b]	2.0332	1.1553
	$r_m^{(2)}$ [b]	2.0312	1.1603
	r_e (this work) [c]	2.0299	1.1632
	r_e^{SE} (this work) [d]	2.0289	1.1632
AuCN	r_0 [b]	1.9125	1.1586
	r_s [b]	1.9123	1.1587
	r_e (this work) [c]	1.9071	1.1623
	r_e^{SE} (this work) [d]	1.9094	1.1620

[a] Experimental values from Ref. 6.

[b] Experimental values from Ref. 7.

[c] Best ab initio values from the composite PES.

[d] Semi-experimental value obtained by combing the ab initio vibration-rotation interaction constants (Table IV) from the composite PESs with the experimental ground state rotational constants.

Tables VIII. Calculated contributions (in kcal mol^{-1}) to the 0 K atomization energies of CuCN, AgCN, and AuCN. See the text for the definitions of the various terms.

	CuCN	AgCN	AuCN
CCSD(T)-F12b/			
aVDZ	276.86	262.00	265.96
aVTZ	279.26	264.90	268.97
aVQZ	279.76	265.60	269.74
aV5Z*	279.67	265.53	269.75
ΔCV	–2.20	+1.47	+2.46
ΔDK3, Val+CV	–0.37	–1.05	–0.43
Δ(4*f*)	---	---	–2.90
ΔT	–0.76	–0.85	–1.05
Δ(Q)	+1.31	+1.08	+1.24
$\Delta(Q)_{\Lambda}$ [a]	+1.08	+1.01	+1.15
ΔSO	–0.07	–0.04	+1.01
ΔZPE	–4.50	–4.29	–4.63
Final Composite	273.08	261.84	265.45

[a] Not used in the final composite result.

Figure Captions

Figure 1. Vibrational wavefunctions for the (020) and (001) states, θ vs. R_2 (M-C distance in bohr). R(C-N) is fixed to its equilibrium value in each case.

Figure 2. Bending PESs, θ (deg.) vs. R_2 (M-C distance in bohr), of CuCN, AgCN, and AuCN from the final composite PESs with the R(C-N) distances fixed at their equilibrium values. The contours are drawn with a spacing of 500 cm^{-1}.

Figure 3. Simulated vibrational spectra (in cm^{-1}) for CuCN, AgCN, and AuCN at temperatures of 5 and 300 K. A Lorentzian line profile was used with a half-width of 5 cm^{-1}.

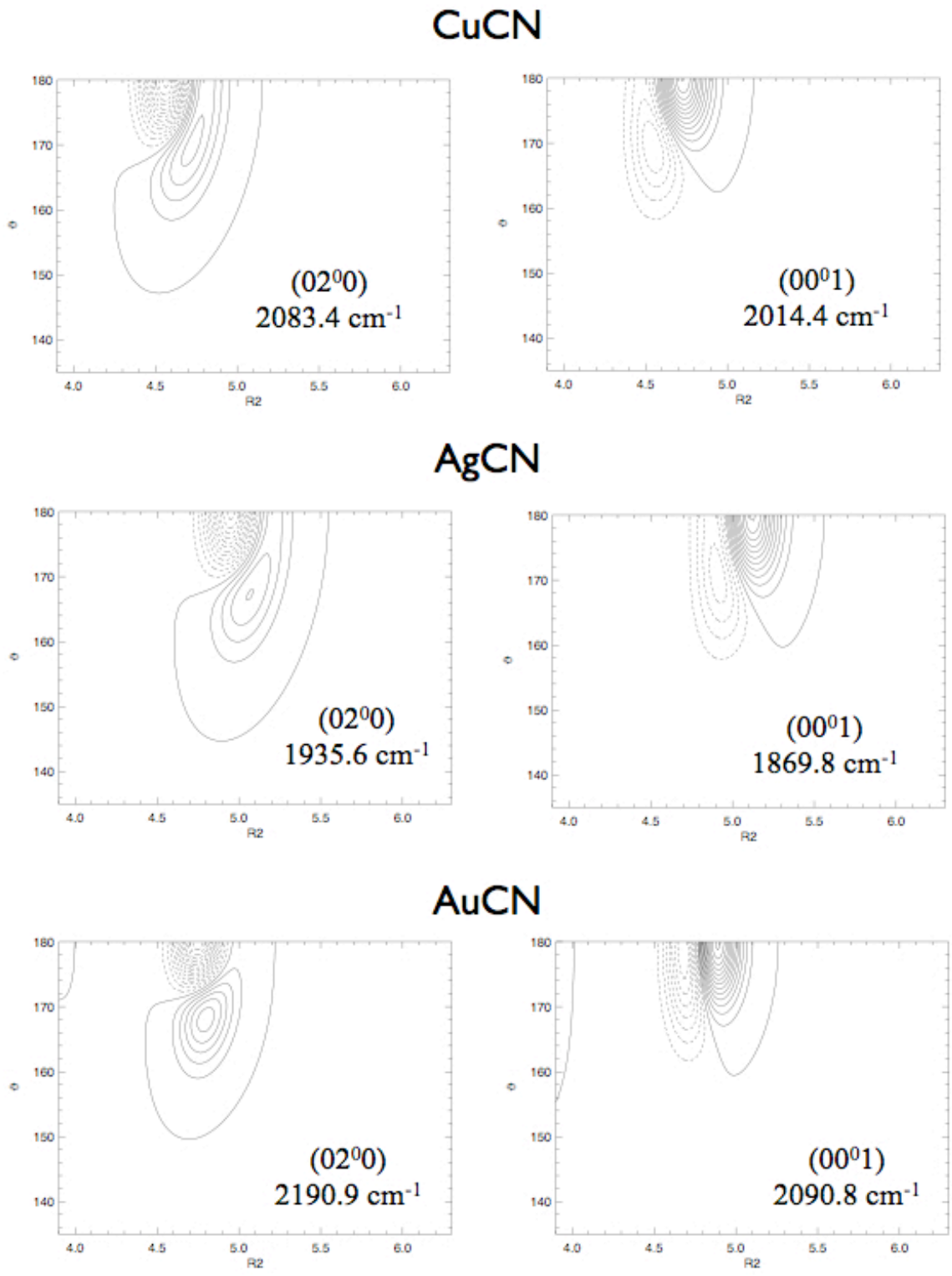
CuCN
(02⁰0)
2083.4 cm-1
(00⁰1)
2014.4 cm-1
AgCN
(02⁰0)
1935.6 cm-1
(00⁰1)
1869.8 cm-1
AuCN
(02⁰0)
2190.9 cm-1
(00⁰1)
2090.8 cm-1
R2

Figure 1.

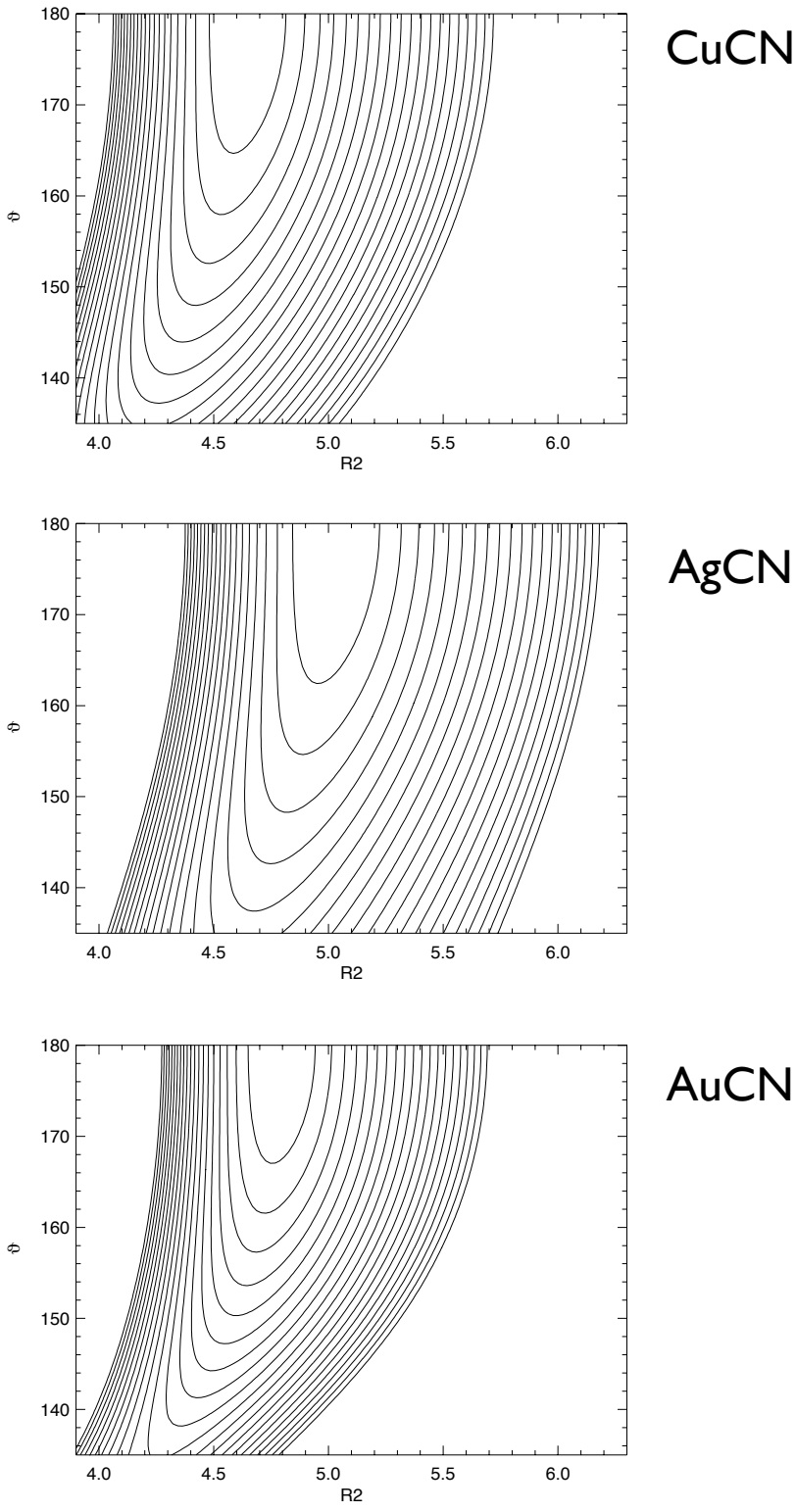

Figure 2.

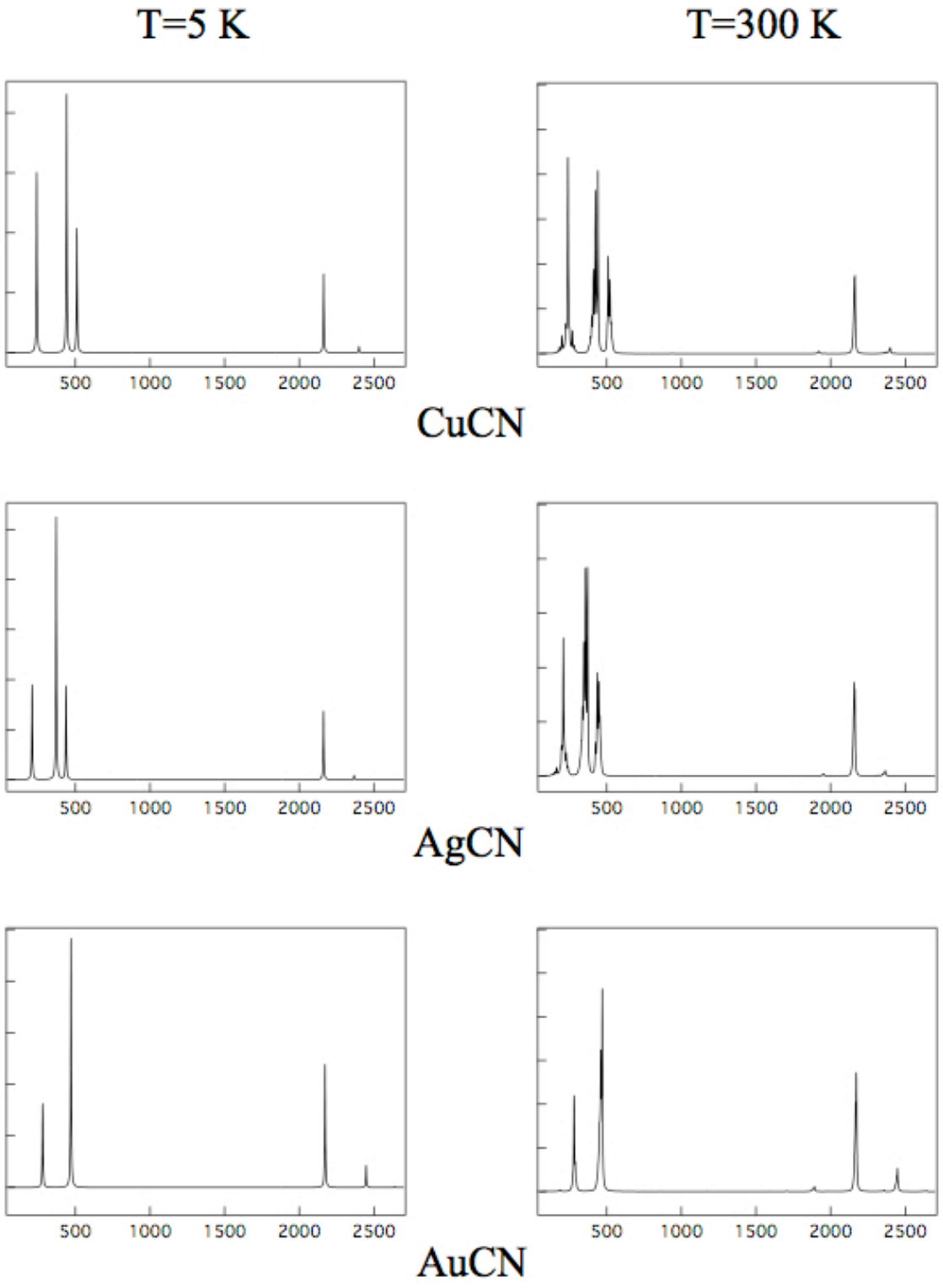

Figure 3.